Experimental Sphere-in-Sphere Testing for the Validation of a Numerical Cerebrospinal Fluid Model

Corina Klug, Wolfgang Sinz, Günter Brenn, Florian Feist *

Abstract The subarachnoid space between skull and brain is filled with Cerebrospinal Fluid (CSF). In most FE head-brain models applied in the field of transport safety, the fluid is modelled as an elastic material with a high bulk and negligible shear modulus. It can be hypothesized that a model considering flow might increase modelling quality of the head-brain interface. In this study, experimental tests were conducted to provide data for the validation of the CSF modelling in an FE code under well-defined and simple boundary conditions, using an artificial CSF and brain surrogates with realistic densities.

Three numerical models were established in LS-DYNA, using either Mat_Elastic_Fluid, Mat_Null with an Equation of State, and Mat_ALE_Incompressible_Fluid for describing the CSF. For a fair comparison, an Arbitrary Lagrangian Eulerian (ALE) discretization was used for all models.

Pressure-time response correlated very well with experimental results for all material models. Relative displacement, though, was not correctly simulated with the commonly used Mat_Elastic_Fluid. Results of experimental tests and numerical simulation were reconfirmed with a simple analytical model. The study showed that brain matter response in FE models, in particular relative displacement, can be considerably improved by applying a correct material model for the CSF.

Keywords ALE, cerebrospinal fluid, experimental testing, simplified FE head model, traumatic brain injury

I. INTRODUCTION

Injuries to the head and traumatic brain injury (TBI) are a significant societal burden. TBI has an 8 times higher annual incidence than breast cancer and 34 times higher annual incidence than HIV/AIDS in the US [1]. According to the WHO European Hospital Morbidity Database, 295 in-patients with intracranial injuries per 100.000 populations have been reported in the year 2010 in Austria. Similar numbers are reported for Germany (286), the Czech Republic (276) and Switzerland (260) [2]. For 30.5% of all injury-related deaths, TBI is a contributing factor. The leading cause of TBI-related deaths is motor vehicle–traffic injury [3].

In legislative and consumer information testing related to transport safety, the head injury criterion (HIC) is commonly used to quantify injury risk to the head. The HIC, established by Versace [4], omits rotations. Attempts to consider rotational loading as well led to criteria like the GAMBIT (Generalized Acceleration Model for Brain Injury Tolerance) [5] and the HIP (Head Impact Power) [6]. These criteria, however, are rarely used and are not applied in legislative or consumer information (e.g. NCAP) testing, since the correlation with real-world injury risk was found to be low and validity has not been entirely proved yet [7], [8], [9].

King et al. [10] suggested using brain response variables (e.g. strain rates) instead of acceleration limits as input-parameters for injury criterions. This gave rise to FE head-brain models to evaluate the effects of combined loading by rotation and translation. Numerous FE head-brain models were developed in the past, which differ in terms of accuracy, level of detail, material models used, and associated parameters [11], [12], [13]. In most FE head-brain models applied in the field of transport safety, the cerebrospinal fluid (CSF) is modelled as an elastic material with high bulk and low shear modulus, e.g. Mat_Elastic_Fluid in LS-DYNA [14]. The CSF fills the gap (subarachnoid space) between skull and brain and protects the latter in case of an impact. Research of D. Pögl showed that depending on age and medical condition the width of the subarachnoid space ranges from 1 to 5 mm.

In the last decades, a significant amount of work has been published on experiments, which can be used for the validation of numerical head-brain models. In post mortem human surrogates (PMHS) [15], [16] and in volunteer tests [17], [18], [19], the mechanical response of the brain to acceleration was investigated. Due to the large number of confounding factors resulting from complex and variable geometry, constraints (falx

*C. Klug is a young researcher and W. Sinz is tenure-track scientist at the Vehicle Safety Institute at Graz University of Technology.
G. Brenn is Dean of Studies, professor and head of Institute for Fluid Mechanics and Heat Transfer at Graz University of Technology.
F. Feist (corresponding author) is senior scientist at the Vehicle Safety Institute at Graz University of Technology (phone: +43/316/873-30312, fax: +43/316/873-30302, email: florian.feist@tugraz.at)

cerebri, fluid reservoir in spinal canal, spinal cord), it is difficult to validate the CSF model based on these experiments. Tests with artificial head-brain models ensure well-defined boundary conditions, but most of the tests in the past were purely two-dimensional and focused on the response of the brain matter rather than on the response of the fluid [20], [21], [22].

The material models Mat_Elastic or Mat_Elastic_Fluid are commonly used in LS-DYNA for modelling the CSF [14]. Baeck et al. [14] compared the response of these material models under simple boundary conditions (i.e. in a cylinder-in-cylinder setup) and showed that the model has a considerable effect on strain energies in the brain matter. The study highlighted the need for a more accurate description of the CSF in FE models. It can be hypothesized that a fluid model considering flow might increase quality and accuracy of FE head-brain models. Starting with release 6, LS-DYNA features such a material model. Mat_ALE_Incompressible_Fluid can simulate the flow of incompressible fluids [23]. It was shown by Aquelet and Souli that this material is able to simulate fluid-structure interaction (FSI) accurately [24].

The aim of the present study is to provide experimental tests for the validation and benchmarking of a numerical fluid material model, considering also the new Mat_ALE_Incompressible_Fluid.

II. METHODS

First, experiments were designed for validating the CSF model in an FE-Code. The experiments featured clear and simple boundary conditions in combination with a limited number of confounding factors, e.g. material parameters of other components like the skull or brain matter. Geometry and materials were selected to allow for a rough comparison with the human head and brain. A sphere-in-sphere model was selected. The brain surrogate was entirely surrounded by the fluid. Dimensions of the brain surrogate and thickness of the fluid layer were selected comparable to those of a healthy adult head-brain.

Second, an analytical model based on the equations of motion for the fluid was established to understand the governing parameters on the pressure in the fluid.

Third, three approaches for modelling the CSF in LS-DYNA were investigated and compared to results obtained in the experimental testing.

Experimental Study

Two near-to-rigid epoxy-resin spheres (diameter 197 mm and 188 mm), as well as one viscoelastic sphere (diameter 188 mm), were used as brain surrogates. Table I lists the main characteristics of the three brain surrogates (denoted as Models A, B and C) used in this study. All materials were selected for their density similar to human brain matter (approx. 1040 kg/m³ [11], [25]). Brain models A and B were made of epoxy resin. Due to the preparation method, the density of Model B was slightly higher than that of Model A.

The viscoelastic sphere (Model C) was made of agar with a concentration of 0.65%, which was found a good brain mimicking material by Deepthi et al. [26] and Pervin et al. [27]. Agar was also used in other studies as a brain model e.g. Takahashi et al. [28] or Kurosawa et al. [29]. Initially, a silicone gel, often used in other studies [20], [22], [30], was applied. However, it was found that this gel is highly sticky and therefore unsuitable for this study. The density of Model C only marginally exceeded the fluid density. However, all brain models were not floating in the CSF, which is also the case for brain matter [31].

TABLE I
PHYSICAL BRAIN MODELS

Surrogate brain	*Material for inner sphere*	*Density*	*E-Modulus*	*Diameter*
		[kg/m³]	[N/mm²]	[mm]
Model A	Epoxy resin	1090	2800	197
Model B	Epoxy resin	1150	2800	188
Model C	Agar gel	1007	-	188
Human brain [31]		1040		

The surrogate brains A, B and C were alternately placed in a translucent spherical shell (inner diameter 200 mm, thickness 7 mm). The gap between inner and outer sphere (1.5 mm for A and 6 mm for B and C) was filled with artificial CSF (aCSF), containing mineral salts, phosphates and proteins realistic in terms of concentration for human adult CSF. The aCSF was prepared as described by Alzet [32]. In brief, a solution A containing the mineral salts, and a solution B containing the phosphates were combined in a 1:1 ratio, and bovine albumin was added. It has to be emphasized that bicarbonate was not added to the compound, since bubbles can develop (see the section 'Discussion' for the effects of bicarbonate in CSF). Table II shows a comparison of artificial and human CSF ingredients concentrations.

TABLE II
COMPOSITION OF ARTIFICIAL CSF AND HUMAN CSF

Component	*Unit*	*Human Cerebrospinal Fluid* [33]	*Artificial Cerebrospinal Fluid* [32]
Na^+	[mM]	150	150
K^+	[mM]	2.9	3.0
Ca^{2+}	[mM]	1.2	1.4
Mg^{2+}	[mM]	1.1	0.8
PO_4^{3-}	[mM]	0.5	1.0
Cl^-	[mM]	120	155
HCO_3^-	[mM]	25	--
Albumin	[g/l]	0.1-0.3	0.3

The test-setup was designed to simulate a fall with pre-acceleration before impact. The model was fixed to a linear guided sled (Fig. 1) and was accelerated with approx. 1 g (pure translation) to 6.4 m/s (LS) or 8.9 m/s (HS). By impacting pre-crushed honeycombs, the sled was decelerated at a near-to-constant 45 g (Fig. 2). The pressure-time response was recorded at 20 kHz at seven circumferential positions (frontal sensors f1 and f2, basal sensors b1 and b2, lateral sensors l1 and l2) – (Fig. 3). In total 36 tests were conducted, i.e. 2 impact velocities (LS/HS), 3 inner spheres models (A, B and C) and 6 repetitions each. One transducer was placed at the reference position on the coup side (f2). The position of the second pressure transducer was changed with every repetition.

Relative displacement was qualitatively recorded with two high-speed cameras and evaluated with a target tracking software. The acceleration was determined with a one-axial accelerometer, and the sled-velocity prior to impact was visually measured with a third high-speed camera, focused on a millimetre scale fixed to the sled.

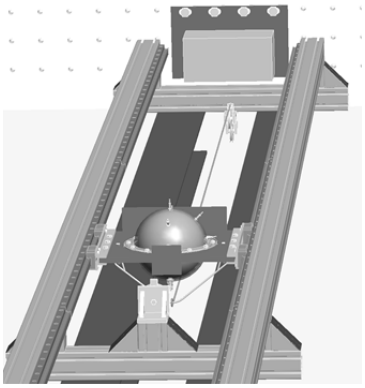

Fig. 1. Experimental sphere-in-sphere model on a linear guided sled

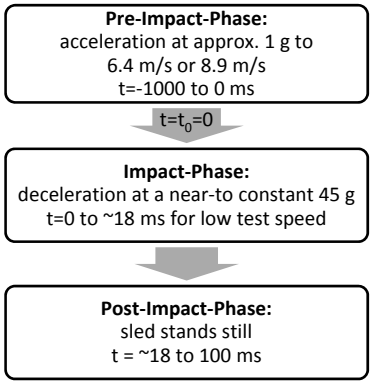

Fig. 2. Test phases

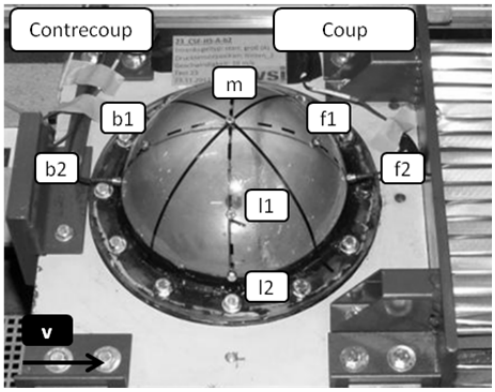

Fig. 3. Experimental sphere-in-sphere model with labelled pressure sensors

Analytical Study

For better understanding the parameters governing the problem, an analytical model was established. This model was derived as follows: the inner sphere representing the brain is immersed in the liquid representing the CSF. Upon acceleration due to an impact, the inner sphere is exposed to a force resulting from the difference of the liquid and sphere densities only. This situation is equivalent to a body floating in a liquid bath under the influence of gravitational acceleration. In cases as the present one, where the sphere and liquid densities differ only slightly, the sphere approximately remains in place relative to the outer shell. This means that the CSF also remains at rest. For this steady-state situation, the equations of motion for the liquid are reduced to the statement that the pressure gradient equals the specific body force due to the acceleration upon impact, i.e.

$$\nabla p = \rho \cdot \vec{a} \tag{1}$$

When the gradient operator is formulated in the spherical coordinates shown in Fig. 4, and the direction of acceleration due to the impact is aligned with the z direction, only one component of the vectorial equation (1) remains. Integration with the assumption of constant fluid density eventually leads to the simple equation

$$p = a \cdot \rho \cdot r \cdot \cos(\theta) \tag{2}$$

where p is pressure, a is acceleration in z-direction, ρ is fluid density and r together with θ are radial and polar angular coordinates of the spherical coordinate system in Fig. 4. In equation (2) the additional constant resulting from the integration was disregarded. This means that the rheological behaviour of the liquid is

assumed irrelevant for the reaction of the system. The shock dampening action of the CSF then is essentially due to buoyancy and not due to viscous or elastic stresses.

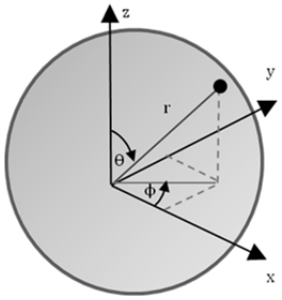

Fig. 4. Spherical coordinates (the loading was aligned with the z-direction)

Numerical Study

Three different numerical models (Table III) for each of the three brain surrogates were created in LS-DYNA version R 6.1. Besides the commonly used Mat_Elastic_Fluid, two alternative material models were applied: Mat_Null with a Grueneisen equation of state (EoS) and Mat_ALE_Incompressible_Fluid. These three approaches are denoted as approaches 1, 2 and 3. Mat_ALE_Incompressible_Fluid was recently added to LS-DYNA for solving computational fluid dynamics (CFD) problems of incompressible fluids [23]. This model implicitly calculates the pressure with the Navier-Stokes and continuity equations using pressure-velocity decoupling [23], [24].

TABLE III
APPROACHES FOR MODELLING THE CSF IN THE NUMERICAL STUDY

Denotation	***Abbreviation***	***Material Model***
Approach 1	ap. 1	MAT_ELASTIC_FLUID
Approach 2	ap. 2	MAT_NULL with EOS_GRUNEISEN
Approach 3	ap. 3	MAT_ALE_INCOMPRESSIBLE_FLUID

An ALE (=Arbitrary Lagrangian Eulerian) formulation was used for all CSF modelling approaches to allow for a fair comparison among them. The ALE mesh was modelled thicker than the initial fluid layer. In other words, the mesh overlapped the inner and outer spheres (Fig. 5). This is essential for the ALE formulation to work. In that way, initially evacuated (void) elements can be filled. This can happen, for example, when the inner sphere moves and unblocks elements which are not initially filled with fluid. The ALE mesh was subdivided in 'inner void', 'fluid' and 'ambient' by means of 'ALE Multi-material groups' (AMMG). Conveniently, the command 'Initial_Volume_Fraction' was used for the filling procedure. Three steps were required: first, the entire ALE mesh was filled with 'void'; second, the entire mesh outside the inner sphere was filled with the 'fluid'; third, the entire mesh outside the outer sphere was filled with 'ambient' (void, vacuum or air). The ALE mesh reference system was attached to the outer sphere. At least three elements discretize the fluid layer in radial direction, which means that in the worst case at least a triangular fluid flow velocity field can be simulated.

Structure parts were discretized with a Lagrangian mesh. The Constrained_Lagrange_in_Solid (CLIS) command was used for the Fluid-Structure Interaction (FSI). A penalty-based compression-/tension-coupling was applied (DIREC=1) with 4-by-4 interaction points per Lagrangian element (NQUAD=4). The FSI allows for free sliding in tangential direction. One CLIS was defined for each applicable interaction pair.

An overview of the numerical model is given in Fig. 5. The outer ring is rigidly connected to a rigid base body at discrete points (bolts). All degrees of freedom (DoF) of the rigid base body (sled) were locked. The entire system is exposed to two acceleration fields, i.e. the gravity and the deceleration pulse (CFC 180 filtered). In approach 2 (Mat_Null with EoS), an ambient pressure of 1.01325 bar was considered.

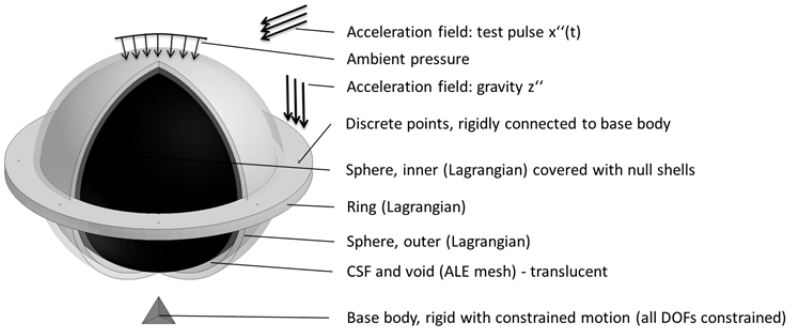

Fig. 5. Summary FE model

In Tables IV and V material models, element forms, cross-sections and material parameters for all three models are summarized. All solids were discretized using hexaeder elements.

In approaches 1 and 2 (Mat_Elastic_Fluid and Mat_Null with EoS), the inner void was modelled with Mat_Vacuum. In the same models, the ambient air was modelled with Mat_Null together with an EoS for the ideal gas. The material parameters for the CSF model of approach 1 were taken from the study of Baeck et al. [14].

In approach 3 (Mat_ALE_Incompressible) only two multi-material groups can be assigned, as only element type 11 (1 point integration with single material and void) can be used. Thus, inner void and ambient were both assigned void. Subsequently, the ambient pressure cannot be assigned in approach 3 and, therefore, only two CLIS cards could be defined. The material parameters for approach 3 were adopted from an example provided by N. Aquelet from LSTC. Values for tolerance of the conjugated gradient were modified, though.

TABLE IV
MATERIALS, MATERIAL MODELS AND ELEMENT FORMS

Part	***Material***	***Material Model***	***Section***
Base	Rigid	Mat_Rigid with centre of mass constraint, prescribed mass and interia velocity	N.a.
Sphere Outer	PET-G	Mat_Piecewise_Linear_Plasticity	Shell, 5pt Integration/Thickness, fully integrated, 6mm
Ring	PET-G	Mat_Piecewise_Linear_Plasticity	Solid, 1pt Integration
Sphere Inner	Epoxy (A,B) OR Agar (C)	Mat_Piecewise_Linear_Plasticity OR Mat_Kelvin-Maxwell_Viscoelastic	Solid, 1pt Integration
Sphere Inner Face	Null	Mat_Null	Shell, 1pt Integration/Thickness, 1pt Integration, 1mm
Void Inner	Vacuum OR Void	Mat_Vacuum (ap. 1,2) OR Mat_ALE_Incompressible (3)	Solid, 1pt Integration (element form 11) (ap. 1,2,3)
Ambient	Air OR Void	Mat_Null with EoS (ap. 1,2)OR Mat_ALE_Incompressible (3)	Solid, 1pt Integration (element form 11) (ap. 1, 2) OR Solid, 1pt Integration (element form 12) (ap. 3)
CSF	CSF	Model 1: Mat_Elastic_Fluid (ap. 1) Model 2: Mat_Null with EoS (ap. 2) Model 3: Mat_ALE_Incompressible (ap. 3)	Solid, 1pt Integration (element form 11) (ap. 1) Solid, 1pt Integration (element form 11) (ap. 2) Solid, 1pt Integration (element form 12) (ap. 3)

In Mat_Null and Mat_ALE_Incompressible, a pressure cut-off (PC) can be defined, in order to simulate spalling (numerical cavitation) of the fluid. In approach 2, PC was assigned -0.1 bar. Considering an ambient pressure of 1.0 bar, this means that tensile stresses of up to 1.1 bar can be transferred from the fluid to the structure. By definition, only negative values can be assigned to the pressure cut-off [34]. Generally, the value should be selected such that the tensile stresses cannot exceed the pressure where cavitation occurs (for water approx. 0.023 bar at 20°C [35]). Selecting the absolute value of the pressure-cut-off-stress too low, though, led to excessive oscillations in the pressure response. The value of -0.1 bar is recommended [36] for water and was found to be a good trade-off between stability, realistic results and little noise in the pressure signal. In approach 3, where no ambient pressure was assigned, PC was consistently assigned -1.1 bar.

To compensate for the ambient pressure in approach 2, an initial energy E_0 was defined in the EoS Model. The Gruneisen Paramters for water were taken from values found in the literature [37].

TABLE V
MATERIAL PARAMETERS

Material	*Density* [kg/mm³]	*Other Material Parameters*
Epoxy	1.15e-6 (A) 1.09e-6 (B)	E=2.8 [GPa], μ=0.3, σ_y=0.048 [GPa], E_{tan}=0.02 [GPa]
PET-G	1.10e-6	E=2.2 [GPa], μ=0.3, σ_y=0.05 [GPa], E_{tan}=0.02 [GPa]
Agar	1.04e-6 (C)	K=1.125 [GPa], G_0=4.9e-5 [GPa], G_I=1.62e-05 [GPa], β=0.145 [1/ms] [38]
Vacuum	1.00e-9	N.a.
Air - EoS	1.205e-9	p_{cut}=-0.0 [GPa], μ=0.0 [GPa.ms], EoS_Ideal_Gas: Cv_0=719 [J/kg.K], Cp_0=1006 [J/kg.K] [37]
CSF (ap. 1)	1.00e-6	K=2.5 [GPa], vc=0.1 [14], IHQ=1, QM=1e-6
CSF (ap. 2)	1.00e-6	p_{cut}=-1.0e-5 [GPa], μ=1.0e-9 [GPa.ms], EoS_Gruneisen: C=1647[mm/ms], S_1=1.921, S_2=-0.096, Γ_0=0.350, E_0=2.895e-4 [J/mm³] - values for water [37], IHQ=1, QM=1e-6
CSF (ap. 3)	1.00e-6	p_{cut}=-1.1e-4 [GPa], μ=1.0e-9 [GPa.ms], Tol=1.0e-9, NCG=20000 , IHQ=1, QM=1e-6

III. RESULTS

Measured pressure-time responses were compared to the analytical model. The relative displacements of inner sphere to outer sphere were qualitatively evaluated. Eventually, the three modelling approaches (1, 2 and 3) were applied to the three models (A, B and C) and compared to experimental data (pressure, displacement). This allowed the identification of drawbacks and benefits of each modelling approach.

Experimental Study

The unfiltered peak pressure over all models was 1.36 bar in Model A at coup position (f2), and -1 bar at contrecoup position (b2) in Model B. Filtering the signals with a CFC 600, the peak coup-pressure dropped to +1.1bar, while the peak contrecoup pressure remained unchanged.

Figs. 6 and 7 show the results for the low-speed tests (6.4 m/s, denoted as LS) and high-speed tests (8.9 m/s, denoted as HS), respectively. All pressure and acceleration signals shown in the figures are CFC 600 filtered.

Both figures a) show the span (minimum, mean, maximum) of the acceleration signal for 18 tests (Model A, B and C). The figures b) show the coup pressure for 6 tests with Model B. The span between maximal and minimal curve is small. Thus, tests were considered highly reproducible with respect to acceleration and pressure.

Evidently, increasing the test velocity led to a longer duration of the acceleration signal but did not affect the pressure and acceleration levels, as the honeycomb provided a constant crush force.

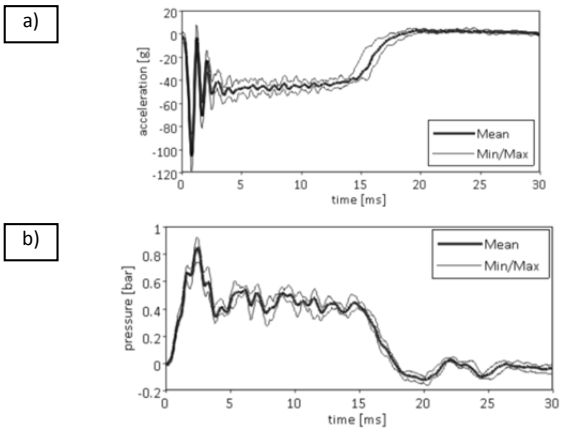

Fig. 6. Acceleration and coup pressure (f2) in Model B atLS

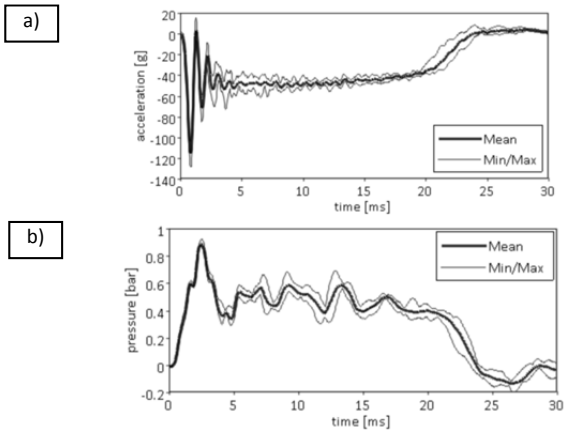

Fig. 7. Acceleration and coup pressure (f2) in Model B at HS

During the impact phase, the displacement of the inner sphere relative to the outer sphere was about 1 mm (±0.5 mm) for the low test speed. (Fig. 8 a and b). Maximal displacement occurred in the post-impact phase (Fig. 8 c), when the outer sphere (the sled) already came to a complete halt. In Fig. 8 b (18 ms after t_0) the sled stands still, but the inner sphere still moves on until the end of the recording at 100 ms (see Fig. 8 c) and reaches values up to 11 mm in Model B (the sphere was not concentric at t0 due to acceleration in the pre-impact phase). The accuracy of the displacement video analysis is limited, because of the limited picture resolution and difficulties with the rotation of the inner sphere.

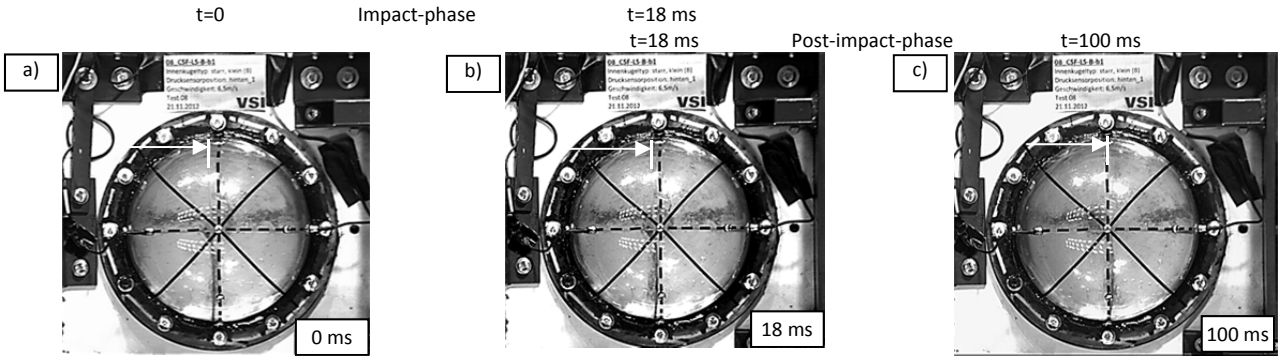

Fig. 8. Displacement of the inner sphere (arrow) relative to the outer sphere (dashed line) at 0, 18 and 100ms after t_0 in a low speed test with model B

Fig. 9 shows the coup pressure response for 3 mm (A) and 6 mm fluid-thickness (B). Peak and increment are higher with the thinner fluid layer. Fig. 10 shows the coup pressure response for elastic (B) and viscoelastic (C) inner sphere. Oscillations in the pressure signal decay more rapidly in the viscoelastic model (C). The curves show the maximum reference pressure of six tests.

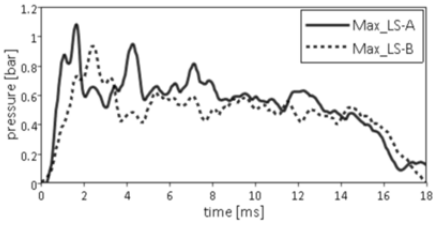

Fig. 9. Comparison between coup pressure of Models A and B at LS

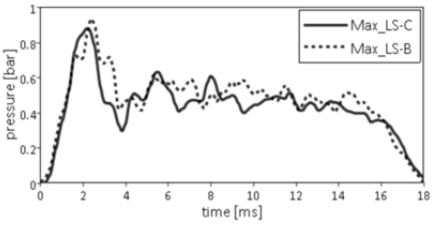

Fig. 10. Comparison between coup pressure of Models B and C at LS

In summary we conclude that results obtained in the experimental study are plausible and were used for a comparison with the numerical model.

Analytical Study

The analytical results were derived by inserting the following values in equation (2): ρ=1000 kg/m³, r=0.1 m and a=45 g, which is the averaged acceleration between t=10 ms and 15 ms. The pressure as a function of circumferential position θ as returned by the analytical model in eq. (2) was compared to experimental results (Fig. 11). The results correlate very well.

Then, the constant acceleration a=45 g was replaced by the measured function of time a=a(t), fixing θ to 10° (reference position). In that way the pressure-time response was calculated (Fig. 12). The pressure rate of change was found considerably higher in the analytical model than in the experiment. After 5 ms, experimental data and analytical results correlate very well. Please refer to the section "Discussion" for a more thorough review of the results.

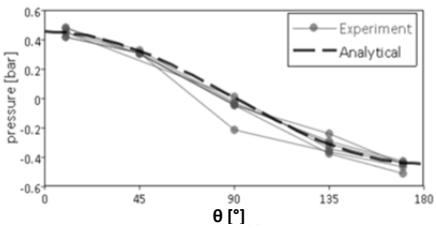

Fig. 11. Pressure as a function of the angle θ: Comparison of analytical and experimental results (average from 10 to 15 ms) – one line per model and speed

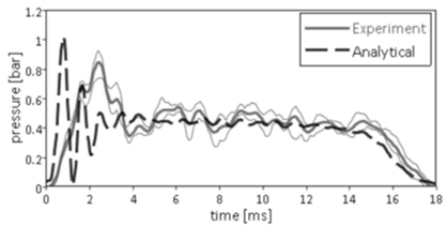

Fig. 12. Pressure at reference position f2 as a function of time t: Comparison of analytical and experimental results (model B, low speed) – experimental sample size: n=6

Numerical Study

The three different CSF modelling approaches (1, 2 and 3) were applied to the three models (A, B and C). Results are summarized in Tables VI through VIII.

With Approach 1, Mat_Elastic_Fluid, the displacement of the inner sphere relative to the outer sphere is dropping to zero immediately after the impact. This is not matching the observations made in the experiments.

With approach 2 and 3 the displacements of model B reach 0.6 mm at the end of the impact, which correlates quite well with the experimental results.

Approach 3, Mat_ALE_Incompressible_Fluid, returned good results in terms of pressure-time response and final displacement. However, when the gap becomes very thin, like in Model A, the solver fails in filling the gap with fluid correctly and the calculation stalls.

Depending on modelling approach, strains and stresses of the inner sphere differ quite significantly. This confirm also the findings by Baeck et al. [14].

In Fig. 14 and 15 the resulting relative displacement of the different approaches is compared to the experimental data. In summary, Mat_Elastic_Fluid completely fails in simulating the displacement of the inner sphere relative to the outer sphere. Results with the other two approaches were satisfying in terms of pressure and displacements immediately after impact. In the post-impact phase, though, also Mat_Elastic_Fluid and Mat_ALE_Incompressible underestimate the total displacement.

Parameter variation showed that the final displacement is depending on various parameters: initial position of the inner sphere, ratio of inner and outer sphere's densities, mesh resolution, fluid gap size and viscosity (Fig. 13).

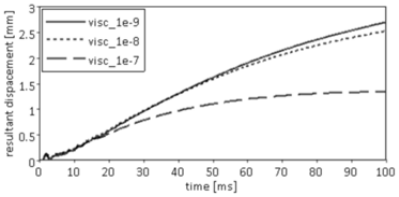

Fig. 13: displacement as a function of viscosity with approach 2(Model B)

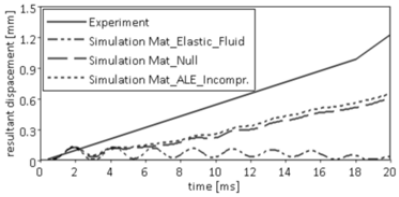

Fig. 14: Comparison of the displacements of different approaches and experiments (±0.5 mm) during the impact phase (Model B)

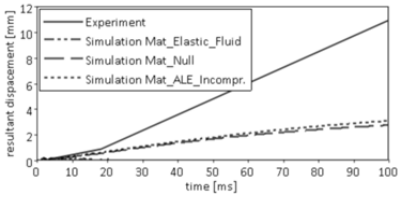

Fig. 15: Comparison of the displacement of different approaches and experiments (±0.5 mm) during the after-impact phase (Model B)

TABLE VI
MODEL A - LARGE NEAR TO RIGID SPHERE

(1) MAT_ELASIC_FLUID	(2) MAT_NULL	(3) MAT_ALE_INCOMPRESSIBLE_FLUID
pressure		
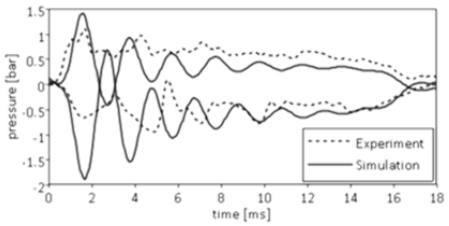	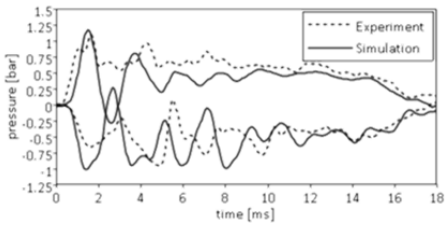	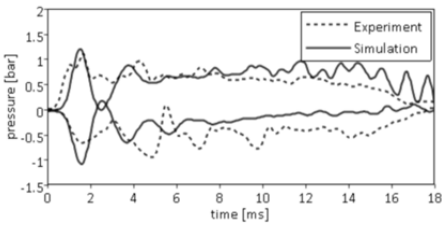
resultant displacement		
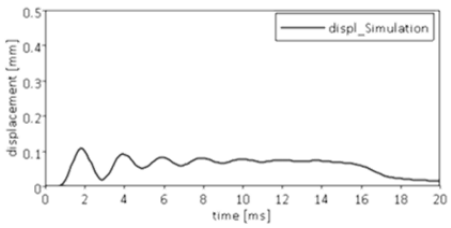	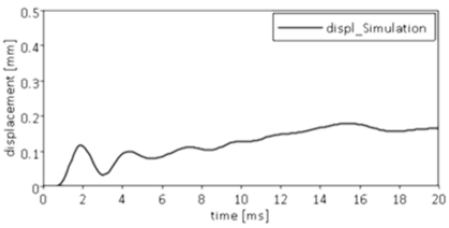	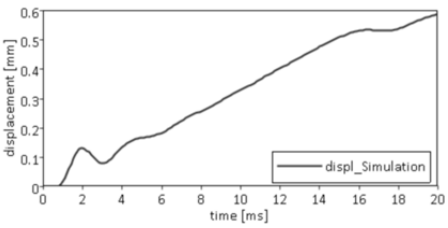
resultant acceleration		
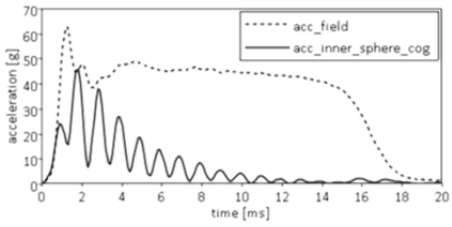	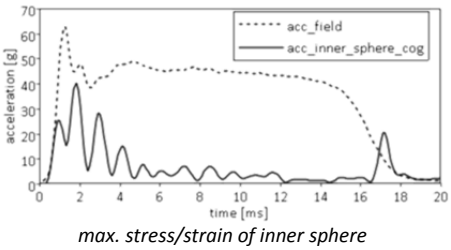	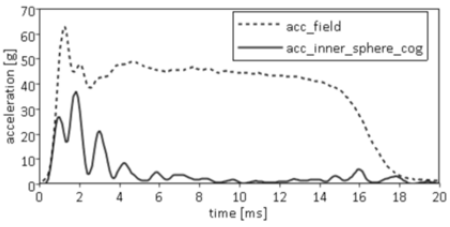
max. stress/strain of inner sphere		
max. effective stress: 154 kPa max. v.m. strain: 4.8E-5 max. internal energy: 1.30E-3	max. effective stress: 112 kPa max. v.m. strain: 3.47E-5 max. internal energy: 1.91 E-3	max. effective stress: 129 kPa max. v.m. strain: 3.94E-5 max. internal energy: 1.57E-3 J

TABLE VII
MODEL B - SMALL NEAR TO RIGID SPHERE

(1) MAT_ELASIC_FLUID	(2) MAT_NULL	(3) MAT_ALE_INCOMPRESSIBLE_FLUID
pressure		
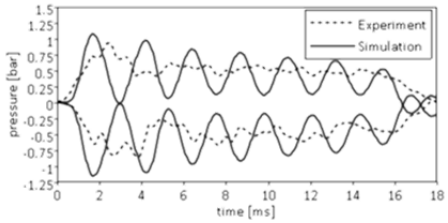	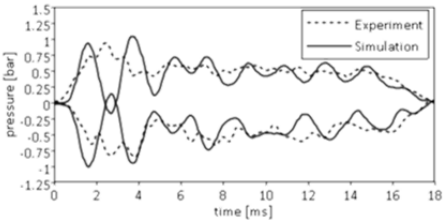	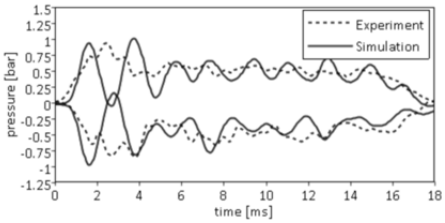
resultant displacement		
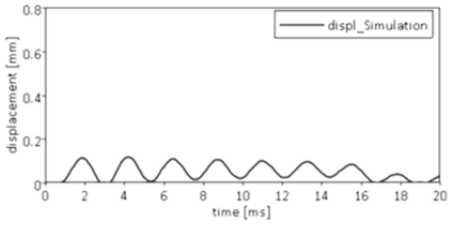	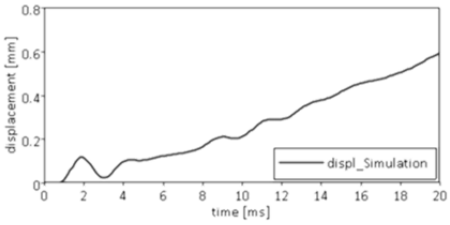	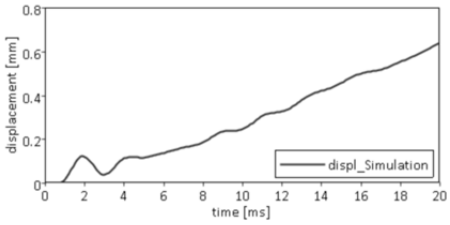
resultant acceleration		
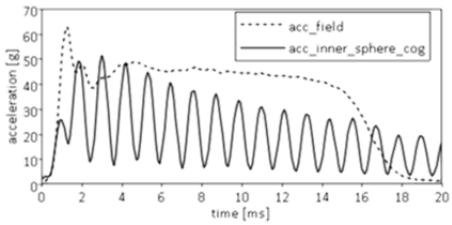	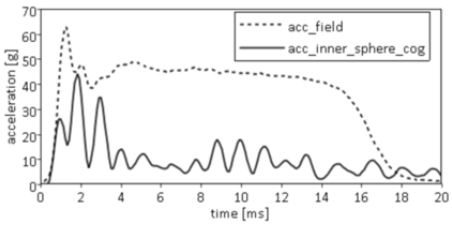	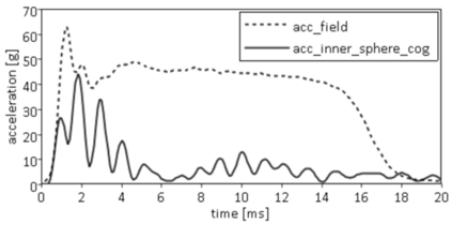
max. stress/strain of inner sphere		
max. von Mises stress: 33 kPa max. von Mises strain: 1.08E-5 max. internal energy: 1.47E-3 J	max. von Mises stress: 141 kPa max. von Mises strain: 4.47E-5 max. internal energy: 3.48E-3 J	max. von Mises stress: 103 kPa max. von Mises strain: 3.24E-5 max. internal energy: 1.24E-3 J

TABLE VIII
MODEL C - SMALL VISCOELASTIC SPHERE

(1) MAT_ELASIC_FLUID	(2) MAT_NULL	(3) MAT_ALE_INCOMPRESSIBLE_FLUID
pressure		
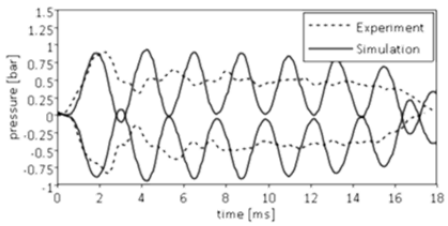	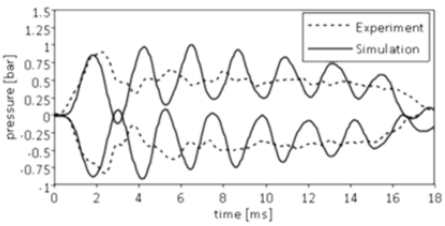	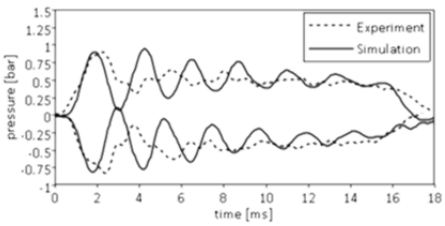
resultant displacement		
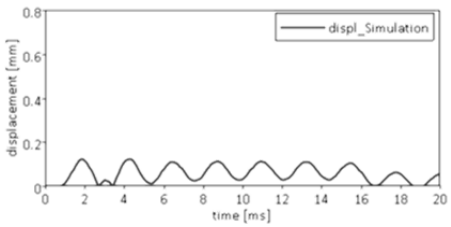	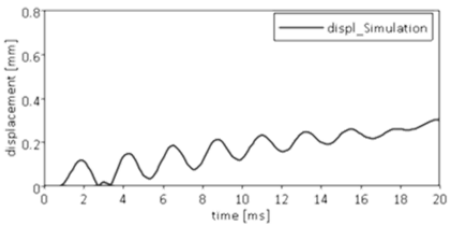	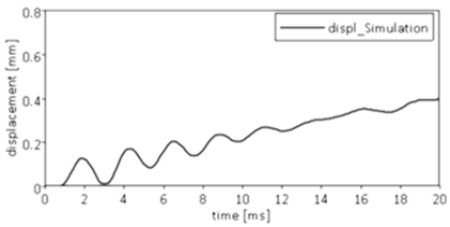
resultant acceleration		
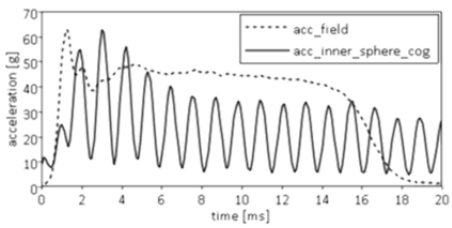	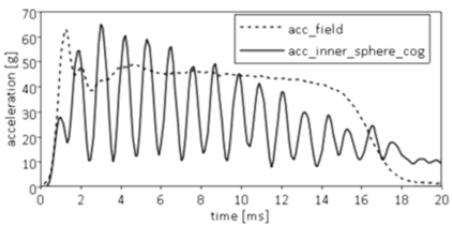	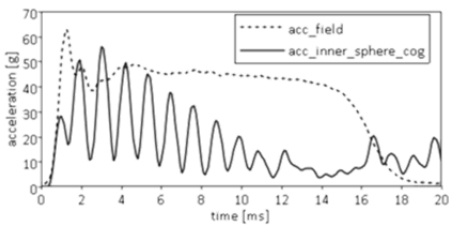
max. stress/strain of inner sphere		
max. von Mises stress: 0.35 kPa max. von Mises strain: 2.67E-3 max. internal energy: 3.45E-3 J	max. von Mises stress: 1 kPa max. von Mises strain: 8.19E-3 max. internal energy: 6.06E-3 J	max. von Mises stress: 2.5 kPa max. von Mises strain: 1.65E-2 max. internal energy: 4.42 E-3 J

Isobaric areas and propagation of pressure waves are influenced by the boundary conditions (Fig. 16). In the present study a solid ring surrounded the outer shell (Fig. 5). In the beginning, an elliptical-shaped isobaric surface can be observed. Later, the pressure waves propagate vertically.

Fig. 16: Propagation of isobaric areas.

IV. DISCUSSION

Experimental Study

The experimental tests showed a high reproducibility. Pre-tests conducted without CSF and inner sphere showed that the pressure transducer signal was not biased by high accelerations. The measured contrecoup pressure of -1 bar (unfiltered) suggests that contrecoup injuries potentially can be caused by cavitation. Goeller et al. found that cavitation within the CSF occurs at negative pressures of about 100 kPa [39], which correlates well with the values assumed in the numerical model.

Experiments showed that the different physical brain models A, B and C differ in terms of pressure-time response: Peak pressure at coup position and the pressure rate of change in the model with the thin fluid layer (A) was higher than with the thicker one (B) – see Fig. 9. Testing with the viscoelastic sphere (C) showed less oscillation in the pressure signal than with the near to rigid ones – see Fig. 10. Although the sphere-in-sphere model is simple, it returned results consistent with PMHS testing. This is shown in Fig. 17, where the linear regression curve of the pressure as a function of acceleration determined by Nahum et al. [16] is compared to the averaged coup pressure determined in the sphere-in-sphere tests.

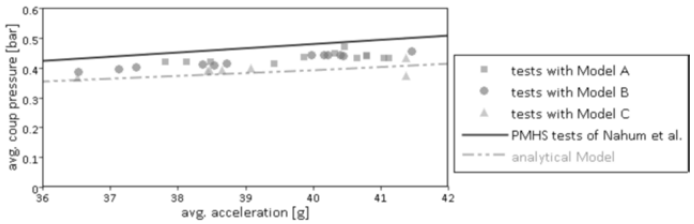

Fig. 17. Comparison between PMHS tests of Nahum et al. [16] and current results for the avg. coup pressure as a function of the avg. acceleration

It was hard to quantify the relative displacement of the inner sphere (Fig. 8). The markings on the inner sphere were hard to track. This applies in particular to model C. Eventually, a reliable quantitative evaluation of the relative displacement between inner and outer sphere could be performed for Model B only.

Nonetheless a qualitative evaluation of the displacement shows that the inner sphere moves on when the outer sphere already stands still.

In the present study, the effect of bicarbonate was not considered in the aCSF. CSF contains approximately 5 times more bicarbonate than tab water [40]. In future studies, the effect of bicarbonate should be investigated. Remarkably, gas bubbles sometimes can be found in MRI/CT scans of patients that sustained a traumatic brain injury, even an open fracture or leakage is not present. It can be argued that such bubbles form due to an increase in CSF reservoir volume, leading to a decrease in CSF pressure. An effect comparable to that known from decompression sickness, where inert gas bubbles form in the tissue due to a rapid reduction in ambient pressure, might lead to this gas-bubble formation. At the same time, this means that contrecoup pressure might be overestimated and coup pressure underestimated in our test setup.

Analytical Study

A reasonable correlation between analytical model, experimental model and PHMS tests by Nahum et al. [16] for the coup pressure was achieved (Fig. 17). Remarkably, both experimental data sets show slightly higher coup pressures than the analytical model. The analytical model does not consider cavitation. Thus, contrecoup pressures are overestimated and coup pressure underestimated.

In the pressure-time response, the analytical model overestimated the pressure increment (Fig. 12). The analytical model does not account for the compliance of structural parts. Thus, pressure rises more rapidly.

In the experimental study it was shown that variation of the test velocity did not affect pressure-level, as the honeycombs provided almost constant crush force. This is evident in the analytical formula as well, where pressure is a function of density, radial and angular position of the sensor, and acceleration.

Very pragmatic assumptions were made in the analytical model: It was assumed that densities of brain matter and fluid are close to equal. Accordingly it was assumed that fluid flow velocity is almost negligible. When disregarding the transient phase, i.e. the initial 5 ms, the close correlation in terms of pressure returned by experiment and analytical formula, shows, that viscosity plays a rather negligible role in the impact phase. Apparently, damping action of the CSF can be reduced to the minor difference in densities.

Numerical Study

The numerical model was investigated for its sensitivity to numerous input parameters. The following observations were made:

Initial position of the inner sphere: The initial position of the inner sphere prior to impact was unknown. An equilibrium position due to an acceleration field of -1 g in x-direction and -1 g in z-direction was assumed as the initial position. A sensitivity study showed that the equilibrium position was a reasonable assumption. An eccentric initial position induced a rotation with up to 25 rad/s² without structure-to-structure contact. The initial position was selected such that at least one element layer of fluid remained between the outer shell and the sphere. Otherwise, LS-DYNA returned unfeasible results, mainly because the void elements did not fill with fluid as soon as the inner sphere separated from the outer sphere. Therefore, it is suggested that a structure-to-structure contact (between inner and outer sphere) is introduced and that contact thickness is selected such that at least one fluid element layer is maintained at all times.

Element size: At least three elements were used for the discretization of the fluid in the radial direction. Doubling the number of elements improved simulation results only marginally. It seems that an accurate fluid flow velocity profile, as provided with a finer mesh, is not essential for the present problem. We did not succeed in introducing a dynamic mesh refine (ALE_refine).

Density of the inner sphere: Increasing the ratio of the sphere and fluid densities led to a larger final displacement. When an inverse ratio was selected, the sphere moved to the contrecoup side. This was simulated correctly with all material models.

Constraints: Propagation of pressure (Fig. 16) shows the effect of the constraint: The outer sphere is surrounded by a ring, stiffening the structure. First, an elliptically shaped pressure ISO surface forms. Later, pressure waves propagate vertically. It therefore can be argued that the structural response of the skull has a considerable effect on peak pressure and propagation. When fully constraining the outer shell, the initial isobaric surface was circular and peak pressure was less local. Later the pressure wave propagated in a ring shape.

Material model for CSF: The numerical models using approaches 2 or 3 returned satisfactory results for pressure of all models and the relative displacement of model B. With approach 3, though, oscillations in the pressure signal decayed more rapidly. The calculation with Mat_ALE_Incompressible_Fluid requires the use of the double precision solver, in particular when selecting a stringent tolerance for the convergence of the conjugate gradient. Also the model did not work with MPP-DYNA. Further, a very conservative time step scaling factor had to be used. Hence, calculation time for approach 3 was by far longer than for the other two.

Penalty Stiffness: Leakage is an issue in Fluid-Structure interaction modelling. Excessively low, as well as excessively high penalty stiffness can lead to leakage. As a result, energy conservation is not met due to sudden development of negative contact energy. A careful selection of the penalty stiffness (with the help of the parameter PFAC) is crucial for fluid-structure interaction modelling. In this study, the penalty stiffness was explicitly defined using a stress-penetration function. Other coupling approaches (constraint-based coupling) were investigated. It was found, though, that energy conservation is also a problem with constrained-based coupling. Another issue intrinsic to the penalty contact, which is generally applied in explicit FEM, is the oscillating pressure response. Such oscillations are found with all three model approaches. In order to reduce the magnitude of oscillations, the acceleration field was filtered at CFC 180 and stiffness-damping (15%) was assigned to all structural materials. The penalty stiffness had also a considerable effect on the magnitude and frequency of the oscillations in the pressure signal.

Ambient Pressure: Approach 2 allows to consider ambient pressure. When doing so, an initial internal energy has to be assigned to the fluid. The effect of ambient pressure was studied. No significant effect for the model under study was observed.

Coefficient of viscosity: A marginal effect of the dynamic viscosity on the inner shell displacement in the impact phase was observed. Viscosity seems rather to have an effect on the post-impact acceleration of the sphere, i.e. the rate of velocity change is larger with higher viscosity – see Fig. 13.

V. CONCLUSIONS

A simple sphere-in-sphere test was created to validate the numerical model of CSF. Compared to PMHS tests, this experimental test setup featured minimal confounding parameters. Compared to other experimental test setups found in the literature, the brain surrogates in our experiments were entirely immersed in a realistic CSF surrogate.

To understand the governing parameters of the problem, an analytical model was established by applying the equations of motion for incompressible fluids.

A numerical model of the problem was created in LS-DYNA. Three different material models were used to describe CSF and compared to the experimental data.

We found that:

- The pressure on the contrecoup side can fall below cavitation pressure. We conclude that cavitation and associated injuries needs to be investigated more thoroughly.
- The effect of the viscosity of the fluid is marginal during the impact phase. This was shown in the analytical and in the numerical models. We conclude that shock dampening of the CSF is essentially due to buoyancy, resulting from the minor difference in densities between brain matter and CSF. Viscous damping plays a role in the post-impact phase, though.
- The kinetics of the brain does not end immediately after the impact. In fact, maximum displacement of the inner sphere (brain) relative to the outer sphere (skull) is reached in the post-impact phase. The post-impact kinetic energy has to be converted to damping and internal energy. Some of this kinetic energy will lead to stretching and – in the worst case – failure of the bridging veins. We conclude that numerical simulation of the head-brain must not end with the impact phase when the strains of the bridging veins are used as an injury criterion. We further conclude that post-impact velocity of the brain relative to the skull is a key parameter for the development of injuries.
- The best correlation between numerical simulation and experiments was achieved with the CSF described by Mat_ALE_Incompressible_Fluid and Mat_Null: The pressure-time response, as well as final relative displacement, did match fairly well. A drawback of the material model Mat_ALE_Incompressible_Fluid, though, is 'leakage'. To prevent leakage, the penalty stiffness and the time step must be selected with care. We conclude that, in order to understand and study the development of subdural haematomas, which are mainly caused by ruptures of the bridging veins, it is important to use a material model for the CSF that is able to simulate relative displacements realistically. Thus, the performances of these two alternatives to the commonly used Mat_Elastic_Fluid have to be investigated in a detailed 3D-FE head-brain model in future studies.
- The isobaric areas and propagation of pressure waves depend on the boundary conditions (in the present study, the skull surrogate was surrounded by a solid ring). We conclude that the impact location has a significant influence on local pressure and pressure propagation. This means that a rigid skull, as assumed sometimes in FE head-brain models, can lead to wrong conclusions. This finding may have also an effect for future development of helmets (spreading the impact load over a larger area).

The most recent version of LS-DYNA (R 7), which was issued in March 2013 (by the time of writing this), offers extended capabilities to simulate incompressible fluid flows.[41] The new incompressible computational fluid dynamics (ICFD) solver will likely help to improve the CSF model further. It is planned that the validated CSF model will be included in a detailed and geometrically correct FE head-brain model. Eventually, the validated CSF model will help to gain more insight into the development and mechanics of traumatic brain injury.

VI. ACKNOWLEDGEMENT

We thank Michael Bottlang, PhD and Dr.med. Dieter Pögl for insightful discussions and comments. We further thank Univ.-Prof. Dipl.-Ing. Dr.techn. Hermann Steffan for providing the temporary funding for this project.

VII. REFERENCES

[1] A Comparison of Traumatic Brain Injury and Leading Injuries or Diseases, *Brain Injury Association of America*, 2004.

[2] European detailed mortality database (DMDB) Copenhagen, *WHO Regional Office for Europe*, 2013

[3] Faul M, Xu L, Wald MM, and Coronado VG, Traumatic Brain Injury in the United States: Emergency Department Visits, Hospitalizations and Deaths 2002 – 2006, *National Center for Injury Prevention and Control, Centers for Disease Control and Prevention*, Atlanta (GA), 2010.

[4] Versace J, A Review of the Severity Index, *SAE International*, Warrendale, PA, 1971.

[5] Newman JA, A generalized acceleration model for brain injury threshold (GAMBIT), *Proceedings of the International IRCOBI Conference 1986*, Zürich, pp. 121–131, 1986.

[6] Newman JA, Shewchenko N, and Welbourne E, A proposed new biomechanical head injury assessment function - the maximum power index, *Stapp Car Crash Journal*, 44:215–247, 2000.

[7] Schmitt K-U, Niederer PF, Muser MH, and Walz F, Trauma Biomechanics: Introduction to Accidental Injury, *Springer*, Berlin Heidelberg New York, 2010.

[8] Feist F, Gugler J, Arregui-Dalmases C, del Pozo de Dios E, López-Valdés F, Deck C, and Willinger R, Pedestrian Collisions with Flat-Fronted Vehicles: Injury Patterns and Importance of Rotational Accelerations as a Predictor for Traumatic Brain Injury (TBI), *Proceedings of the 21st International Technical Conference on the Enhanced Safety of Vehicles*, Stuttgart, Germany, pp. 1–19, 2009.

[9] Marjoux D, Baumgartner D, Deck C, and Willinger R, Head injury prediction capability of the HIC, HIP, SIMon and ULP criteria, *Accident Analysis & Prevention*, 40(3):1135–1148, 2008.

[10] King AI, King HY, Zhang L, and Hardy W, Is head injury caused by linear or angular acceleration?, *Proceedings of the IRCOBI Conference 2003*, Lisbon, pp. 1-12, 2003.

[11] Deck C, and Willinger R, Head injury prediction tool for protective systems optimisation, *Proceedings of the 7th European LS-DYNA Conference*, Salzburg, 2009.

[12] Horgan TJ, and Gilchrist MD, The creation of three-dimensional finite element models for simulating head impact biomechanics, *International Journal of Crashworthiness*, 8(4):353–366, 2003.

[13] Kleiven S, Evaluation of head injury criteria using a finite element model validated against experiments on localized brain motion, intracerebral acceleration, and intracranial pressure, *International Journal of Crashworthiness*, 11(1):65–79, 2006.

[14] Baeck K, Goffing J, and Vander Sloten J, The use of different CSF representations in a numerical head model and their effect on the results of FE head impact analyses, *Proceedings of the 8th European LS-DYNA Users Conference*, Strasbourg, 2011.

[15] Hardy WN, Mason MJ, Foster CD, Shah CS, Kopacz JM, Yang KH, King AI, Bishop J, Bey M, Anderst W, und Tashman S, A Study of the Response of the Human Cadaver Head to Impact, *Stapp Car Crash Journal*, 51:17–80, 2007.

[16] Nahum AM, Smith R, and Ward CC, Intracranial Pressure Dynamics During Head Impact, *Proceedings of the 21st Stapp Car Crash Conference,* SAE paper no. 770922*,* Warrendale, PA, pp. 339-366, 1977.

[17] Bayly PV, Cohen TS, Leister EP, Ajo D, Leuthardt E, and Genin GM, Deformation of the human brain induced by mild acceleration, *Journal of Neurotrauma*, 22(8):845–856, 2005

[18] Sabet AA, Christoforou E, Zatlin B, Genin GM, and Bayly PV, Deformation of The Human Brain Induced By Mild Angular Head Acceleration, *Journal of Biomechanics*, 41(2):307–315, 2008.

[19] Feng Y, Abney TM, Okamoto RJ, Pless RB, Genin GM, and Bayly PV, Relative brain displacement and deformation during constrained mild frontal head impact, *Journal of The Royal Society Interface*, 7(53):1677-1688, 2010.

[20] Brands DWA, Bovendeerd PHM and Wismans JSHM, On the potential importance of non-linear viscoelastic material modelling for numerical prediction of brain tissue response: test and application, *Stapp Car Crash Journal*, 46:103–121, 2002.

[21] Ivarsson J, Viano DC, Lövsund P, and Aldman B, Strain relief from the cerebral ventricles during head impact: experimental studies on natural protection of the brain, *Journal of Biomechanics*, 33(2):181–189, 2000.
[22] Bradshaw DRS, Ivarsson J, Morfey CL, and Viano DC, Simulation of acute subdural hematoma and diffuse axonal injury in coronal head impact, *Journal of Biomechanics*, 2001, 34(1):85–94.
[23] Souli M, ALE Incompressible Fluid in LS-DYNA, *Proceedings of the 11th International LS-DYNA Users Conference*, Detroit, 2010.
[24] Aquelet N, and Souli M, ALE incompressible Fluid in LS-DYNA, *Proceedings of the 12th International LS-DYNA Conference*, Detroit, 2012.
[25] Kleiven S, Predictors for traumatic brain injuries evaluated through accident reconstructions, *Stapp Car Crash Journal*, 51:81–114, 2007.
[26] Deepthi R, Bhargavi R, Jagadeesh K, and Vijaya MS, Rheometric studies on agarose gel- a brain mimic material, *SASTECH Journal*, 9(2):27-30, 2010.
[27] Pervin F, and Chen WW, Mechanically Similar Gel Simulants for Brain Tissues, in Dynamic Behavior of Materials, *Proceedings of the Society for Experimental Mechanics Series Conference*, pp. 9-13, 2011.
[28] Takahashi T, Kato K, Ishikawa R, Watanabe T, Kubo M, Uzuka T, Fujii Y, and Takahashi H, 3-D finite element analysis and experimental study on brain injury mechanism, *Proceedings of the 29th Annual International Conference of the IEEE EMBS*, Lyon, pp. 3613–3616, 2007.
[29] Kurosawa Y, Kato K, Saito S, Kubo M, Uzuka T, Fujii Y, and Takahashi H, Basic study of brain injury mechanism caused by cavitation, *Proceedings of the 31st Annual International Conference of the IEEE EMBS,* Minneapolis, pp. 7224–7227, 2009.
[30] Viano D, Aldman B, Pape K, van Hoof J, and von Holst H, Brain kinematics in physical model tests with translational and rotational acceleration, *International Journal of Crashworthiness*, 2(2):191–206, 1997.
[31] Bilston LE, Neural Tissue Biomechanics, pp. 122, *Springer*, Berlin Heidelberg, 2011.
[32] Durect Corporation- Alzet, "Preparation of Artificial CSF" Internet: [http://alzet.com/products/guide_to_use/cfs_preparation.html], 2013 [Accessed: 28-Mar-2013].
[33] Löffler G, Basiswissen Biochemie: mit Pathobiochemie, pp. 471, *Springer*, Heidelberg, 2008.
[34] LSTC, LS-DYNA Keyword User's Manual Volume I Version 971 R6.1.0, Livermore, 2012.
[35] Kell GS, Density, Thermal Expansivity, and Compressibility of Liquid Water from 0° to 150°C: Correlations and Tables for Atmospheric Pressure and Saturation Reviewed and Expressed on 1968 Temperature Scale, *Journal of Chemical and Engineering Data*, 20(1):97–105, 1975.
[36] Olovsson L, Souli M, and Do I, LS-DYNA – ALE Capabilities (Arbitrary-Lagrangian-Eulerian) Fluid-Structure-Interaction Modeling, 2003.
[37] Do I, and Day J, Overview of ALE Method in LS-DYNA, 2005.
[38] Tinard V, Deck C, and Willinger R, New methodology for improvement of helmet performances during impacts with regards to biomechanical criteria, *Materials & Design*, 37:79–88, 2012.
[39] Goeller J, Wardlaw A, Treichler D, O'Bruba J, and Weiss G, Investigation of cavitation as a possible damage mechanism in blast-induced traumatic brain injury, *Journal of neurotrauma,* 29(10):1970–1981, 2012.
[40] Judd S, Process Science and Engineering for Water and Wastewater Treatment, pp. 48, *IWA Publishing*, London, 2002.
[41] Del Pin F, and Çaldichoury I, LS-DYNA® 980 : Recent Developments, Application Areas and Validation Process of the Incompressible fluid solver (ICFD) in LS-DYNA, *Proceedings of the 12th International LS-DYNA Conference*, Detroit, 2012.